Elucidating the Limit of Li Insertion into the Spinel Li$_4$Ti$_5$O$_{12}$

Haodong Liu,[†,∇] Zhuoying Zhu,[†,∇] Jason Huang,[†,∇] Xin He,[‡] Yan Chen,[§] Rui Zhang,[⊥] Ruoqian Lin,[∥] Yejing Li,[†] Sicen Yu,[†] Xing Xing,[†] Qizhang Yan,[†] Xiangguo Li,[†] Matthew J. Frost,[§] Ke An,[§] Jun Feng,[‡] Robert Kostecki,[‡] Huolin Xin,*,[⊥] Shyue Ping Ong,*,[†,#] and Ping Liu*,[†,#]

[†]Department of Nanoengineering, University of California, San Diego, California 92093, United States

[‡]Energy Storage and Distributed Resources Division, Lawrence Berkeley National Laboratory, Berkeley, California 94720, United States

[§]Neutron Scattering Division, Oak Ridge National Laboratory, Oak Ridge, Tennessee 37830, United States

[⊥]Department of Physics and Astronomy, University of California, Irvine, California 92697, United States

[∥]Chemistry Division, Brookhaven National Laboratory, Upton, New York 11973, United States

[#]Sustainable Power and Energy Center, University of California San Diego, La Jolla, California 92093, United States

Ⓢ *Supporting Information*

ABSTRACT: In this work, we show that the well-known lithium-ion anode material, Li$_4$Ti$_5$O$_{12}$, exhibits exceptionally high initial capacity of 310 mAh g^{-1} when it is discharged to 0.01 V. It maintains a reversible capacity of 230 mAh g^{-1}, far exceeding the "theoretical" capacity of 175 mAh g^{-1} when this anode is lithiated to the composition Li$_7$Ti$_5$O$_{12}$. Neutron diffraction analyses identify that additional Li reversibly enters into the Li$_7$Ti$_5$O$_{12}$ to form Li$_8$Ti$_5$O$_{12}$. density functional theory (DFT) calculations reveal the average potentials of the Li$_4$Ti$_5$O$_{12}$ to Li$_7$Ti$_5$O$_{12}$ step and the Li$_7$Ti$_5$O$_{12}$ to Li$_8$Ti$_5$O$_{12}$ step are 1.57 and 0.19 V, respectively, which are in excellent agreement with experimental results. Transmission electron microscopy (TEM) studies confirm that the irreversible capacity of Li$_4$Ti$_5$O$_{12}$ during its first cycle originates from the formation of a solid electrolyte interface (SEI) layer. This work clarifies the fundamental lithiation mechanism of the Li$_4$Ti$_5$O$_{12}$, when lithiated to 0.01 V vs Li.
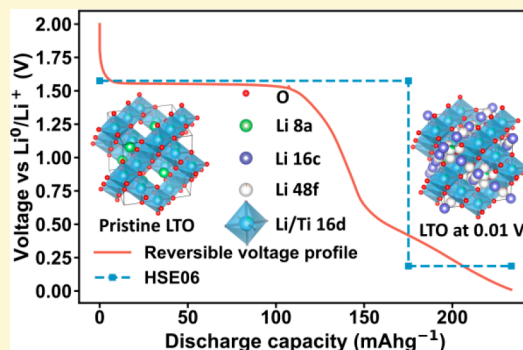
Li$_4$Ti$_5$O$_{12}$ (LTO) is a well-known anode material for long-life, high rate Li-ion batteries. Its high stability, excellent safety, and outstanding rate capability have led to its successful commercialization.[1−7] LTO, or [Li$_3$]^{8a}[Li$_1$Ti$_5$]^{16d}[□]^{16c}[O$_{12}$]^{32e} possesses a spinel structure with the $Fd\overline{3}m$ space group. Regarding the lithiation mechanism, it is widely accepted that it takes 3 Li$^+$ per formula unit to form [□]^{8a}[Li$_1$Ti$_5$]^{16d}[Li$_6$]^{16c}[O$_{12}$]^{32e}.[8] Accordingly, the theoretical capacity of LTO is calculated to be 175 mAh g^{-1}. Its operating potential is ~1.5 V vs Li/Li$^+$. However, the process of Li$^+$ intercalation into the Li$_4$Ti$_5$O$_{12}$ to form Li$_7$Ti$_5$O$_{12}$ only reduces 60% of the Ti^{4+} in the crystal to the Ti^{3+}. If assuming fully utilization of the Ti^{3+}/Ti^{4+} redox, the Li$_7$Ti$_5$O$_{12}$ is able to take an additional 2 Li$^+$ to form Li$_9$Ti$_5$O$_{12}$. As well agreed from a structural point of view, there are additional vacancies to host up to 3 extra Li$^+$ at the 8a sites per unit cell to form Li$_9$Ti$_5$O$_{12}$ or even Li$_{10}$Ti$_5$O$_{12}$. In principle, LTO has the capability to host more than 3 Li$^+$ per formula, which will greatly boost the capacity in the LTO anode.

Since the Li$_7$Ti$_5$O$_{12}$ was treated as the discharge product of the LTO, earlier reported works usually discharged the LTO to 1 V.[9] There have been several reports of cycling LTO to lower potentials. Yi cycled the LTO between 0.01 and 2.5 V and reported a first-cycle discharge capacity of 270 mAh g^{-1} with a reversible capacity of 210 mAh g^{-1}.[10−12] Wang employed atomic-resolution annular bright-field imaging and electron energy-loss spectroscopy to measure local Li occupancy of LTO at 0.01 V. They observed partial re-occupation of 8a sites by further lithiation of Li$_7$Ti$_5$O$_{12}$, and claimed that the increased capacity in LTO is due to the extra storage of Li in the near-surface region.[13] However, the microscopy-based study mainly represents the general lithiation mechanism in the localized surface of LTO. Ge investigated the structural evolution of LTO between 0.01 and 2.5 V via in situ X-ray
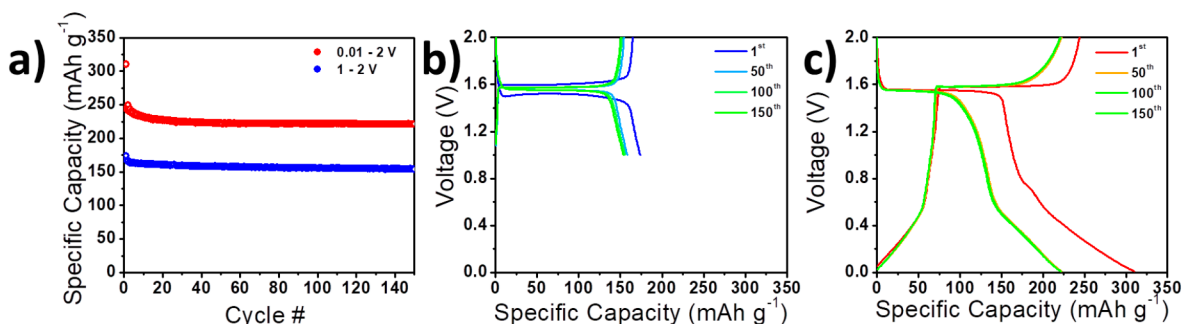
Figure 1. Comparison of electrochemical performance of LTO discharged to different voltages: (a) capacities and (b and c) voltage profiles over the course of 150 cycles at 20 mA g^{-1}.
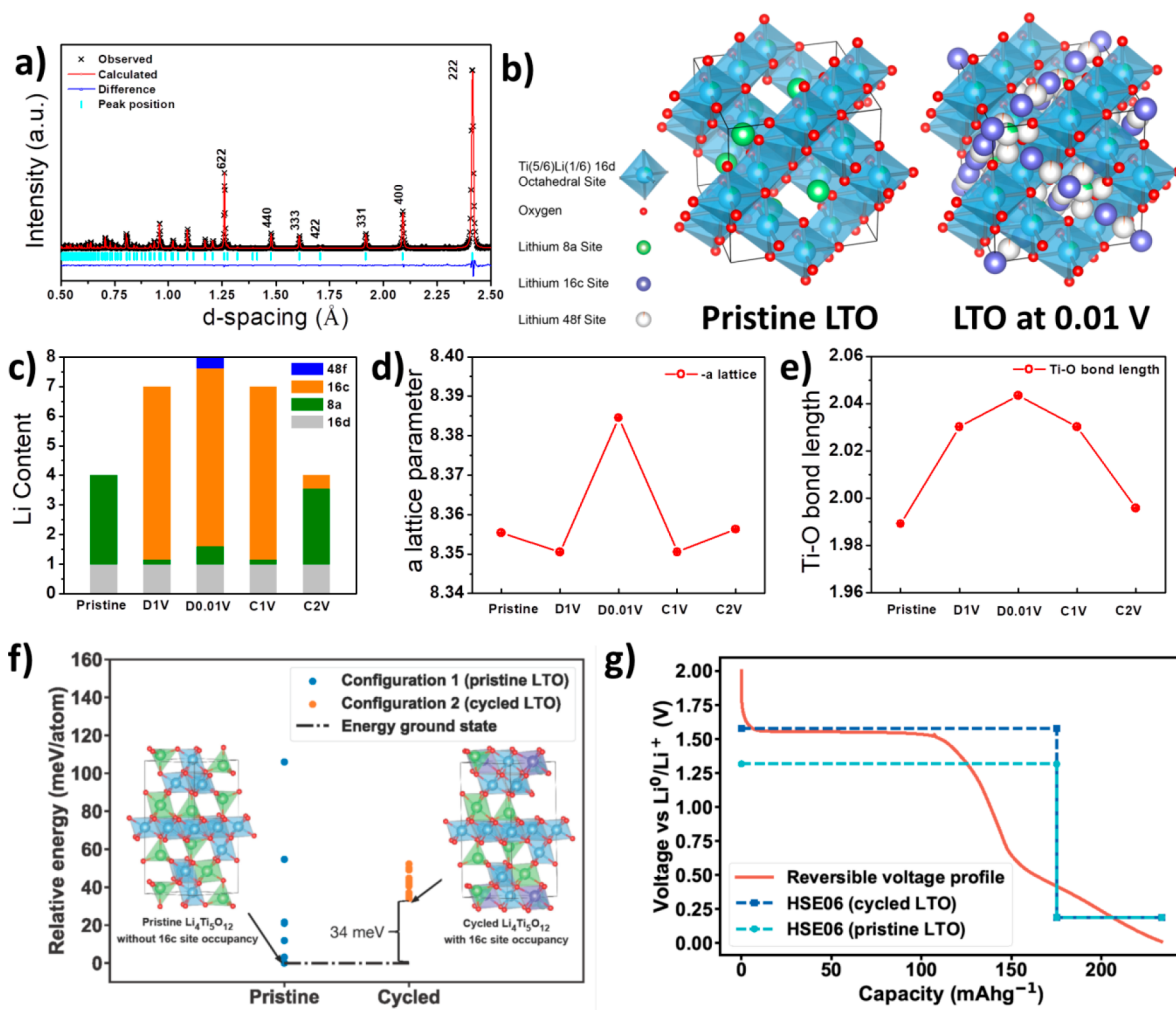

Figure 2. Crystal structure analysis of LTO at different states of (dis)charge via neutron diffraction: (a) neutron diffraction refinement of pristine LTO, (b) crystal structure of pristine LTO and LTO at 0.01 V on first discharge, (c) Li site occupancies at different states of (dis)charge, (d) lattice parameters, (e) Ti−O bond lengths, (f) relative energy for different orderings of pristine and cycled Li$_4$Ti$_5$O$_{12}$, (g) voltage profiles of simulated curves using HSE06 functional (with pristine/cycled state of Li$_4$Ti$_5$O$_{12}$) and reversible experimental capacity after stable SEI formation.

diffraction (XRD).[14] Because of the low scattering power of Li, their XRD refinement results qualitatively indicated the 8a sites of LTO could host the extra Li in the bulk. Despite of these investigations, two outstanding questions regarding the (de)lithiation mechanism of LTO still have not been resolved yet:

(1) How much Li$^+$ could reversibly enter into LTO, and how are the Li$^+$ cations distributed at different sites?

(2) What causes the first cycle irreversible capacity of LTO discharged to 0.01 V?

In this work, we discharged and charged the LTO between 0.01 V and 2.0 V at first. The LTO delivered an initial discharge capacity of 310 mAh g^{-1} and showed a reversible
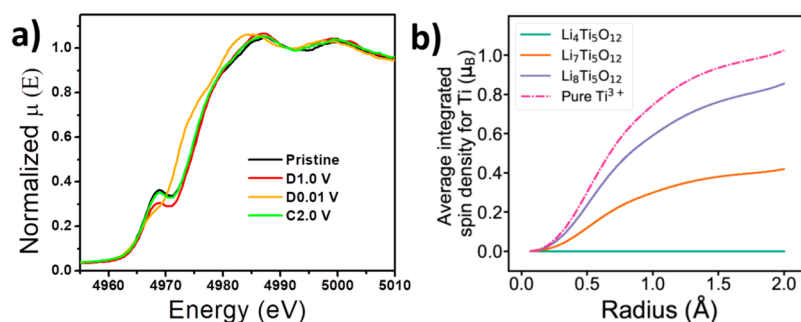
Figure 3. Charge compensation mechanism of LTO: (a) the Ti K-edge at different states of (dis)charge, and (b) average integrated spin density for Ti, as a function of radius from Ti, up to 2 Å.

capacity of 230 mAh g^{-1}. Taking advantage of the high sensitivity of neutron scattering to light elements such as Li,[15,16] we performed Rietveld analysis of neutron powder diffraction data to arrive at a reliable and detailed crystal structural characterization of LTO.[17−20] The Li occupancies at different sites were quantitatively identified. Our DFT calculations not only confirmed the structures of the (de)lithiated LTO, but also explained the voltage profile of the LTO. Finally, a solid electrolyte interface (SEI) layer with a thickness of 12 nm was observed on the surface of the fully discharged LTO, which indicated that the irreversible capacity in the first cycle was associated with the formation of the SEI.

Figure 1 compares the electrochemical performance of the LTO cycled with different voltage windows. Both cells were cycled at a moderate current density of 20 mA g^{-1}. The cell cycled with a cut-off voltage at 1.0 V exhibited an initial discharge capacity of 174 mAh g^{-1}, its capacity was stabilized at 162 mAh g^{-1} after 10 cycles. This performance was consistent with previous reports and corresponded to the process from $Li_4Ti_5O_{12}$ to $Li_7Ti_5O_{12}$.[21] While the cell discharged to 0.01 V delivered an exceptionally high capacity of 310 mAh g^{-1} for its first discharge, its reversible capacity at the 10th cycle was 233 mAh g^{-1}. The LTO displayed excellent cycling stability for both cut-off voltages, indicating the process for the extra lithiation beyond $Li_7Ti_5O_{12}$ is highly reversible. The voltage profiles present three characteristic regions during the first discharge. The long plateau at 1.55 V is associated with the formation of the $Li_7Ti_5O_{12}$. Below 1.0 V, a bump at ∼0.8 V and a slope under 0.6 V are observed. The bump disappeared after the first discharge, suggesting that this electrochemical process is irreversible.

According to the capacity, the LTO takes in 5.3 Li atoms during the first discharge, while only 4 Li atoms reversibly participate in the following cycles. The irreversible Li may either be trapped into the LTO host or be consumed by side reactions. A quantitative analysis of the Li site occupancies in the bulk of LTO at different states of (dis)charge will provide a direct understanding of the extra Li insertion mechanism of the LTO. Neutron diffraction was performed, because of its high sensitivity to Li, on LTO at a series of lithiation states.[17,18] Figure 2a depicts the Rietveld refinement of the neutron diffraction profile of the pristine LTO. Its structure is well-modeled by the spinel phase ($Fd\bar{3}m$).[8] Figure 2b shows the structure of pristine LTO; the 32e sites are fully occupied by O atoms, the 16d sites are shared by Ti and Li at the ratio of 5:1, and the rest of Li fills the 8a sites (noted as $[Li_3]^{8a}[Li_1Ti_5]^{16d}$-$[O_{12}]^{32e}$). Figure 2c summarizes the site occupancies of the Li in the LTO at different states of (dis)charge. The refined

profiles and detailed structure information are presented in the Supporting Information (see Figure S1-5 and Table S1-5). During the long plateau region on discharge, 3 Li atoms enter into LTO at the 16c sites, accompanied by a large amount of the Li transferring from the 8a sites to the 16c sites to form $[Li_{0.16}]^{8a}[Li_1Ti_5]^{16d}[Li_{5.84}]^{16c}[O_{12}]^{32e}$. Further discharge of LTO to 0.01 V only takes 1 Li, which fills the 16c sites first, then distributes between the 8a sites and the 48f sites. The LTO at 0.01 V can be described as $[Li_{0.62}]^{8a}[Li_1Ti_5]^{16d}[Li_6]^{16c}$-$[Li_{0.38}]^{48f}[O_{12}]^{32e}$. Once charged back to 1.0 V, the LTO structure turns into the $[Li_{0.16}]^{8a}[Li_1Ti_5]^{16d}[Li_{5.84}]^{16c}[O_{12}]^{32e}$ again. After one electrochemical cycle, the LTO structure is noted as $[Li_{2.57}]^{8a}[Li_1Ti_5]^{16d}[Li_{0.43}]^{16c}[O_{12}]^{32e}$, suggesting that the Li is extracted from the 16c sites, while a certain amount of Li transfers back to the 8a sites. Significantly, there is Li located at 16c sites in the delithiated LTO, which differs from the pristine LTO. The neutron diffraction refinements identify that 4 Li are reversibly intercalated into the LTO.

Besides the Li occupancies, the crystal lattice changes of LTO are also studied.[19,20] Figure 2d shows that, despite 4 Li atoms entering the crystal, the lattice change of the LTO is very small. The volume of the $Li_7Ti_5O_{12}$ unit cell is only 0.18% smaller than the $Li_4Ti_5O_{12}$, leading to its reputation as a "zero-strain" material.[3,22] The $Li_8Ti_5O_{12}$ shows a 1.08% volume expansion, compared to the $Li_4Ti_5O_{12}$, which is still extremely minor. Figure 2e exhibits the evolution of the Ti−O bond length. At the pristine state, the Ti−O bond length is 1.9892 Å. As 3 Li atoms enter into the LTO, the Ti−O bond increases to 2.0302 Å in $Li_7Ti_5O_{12}$. The $Li_8Ti_5O_{12}$ shows the longest Ti−O bond of 2.0434 Å. The increase of the Ti−O bond indicates the reduction of the Ti caused by the Li insertion. During charging, the Ti−O bond length decreases. The Ti−O bond of $Li_4Ti_5O_{12}$ after one cycle becomes 1.9958 Å, which is slightly larger than that observed in the pristine LTO. This difference may come from the change in Li occupancies at 8a and 16c sites.

We performed DFT calculations using GGA functional[23] on all symmetrically distinct orderings of pristine ($[Li_3]^{8a}[Li_1Ti_5]^{16d}[O_{12}]^{32e}$) and cycled $Li_4Ti_5O_{12}$ ($[Li_{2.5}]^{8a}[Li_1Ti_5]^{16d}[Li_{0.5}]^{16c}[O_{12}]^{32e}$). As shown in Figure 2f, we find that the lowest energy ordering of the cycled material is only 34 meV higher than the lowest energy ordering of the pristine material. This suggests that the metastable state with a small 16c site occupancy is accessible through electrochemical cycling at room temperature.[24]

Figure 2g shows the voltage profile for up to 4 Li atoms inserted into LTO with stable phases at x = 4, 7, 8 in $Li_xTi_5O_{12}$ computed using the HSE06 functional.[25,26] The average
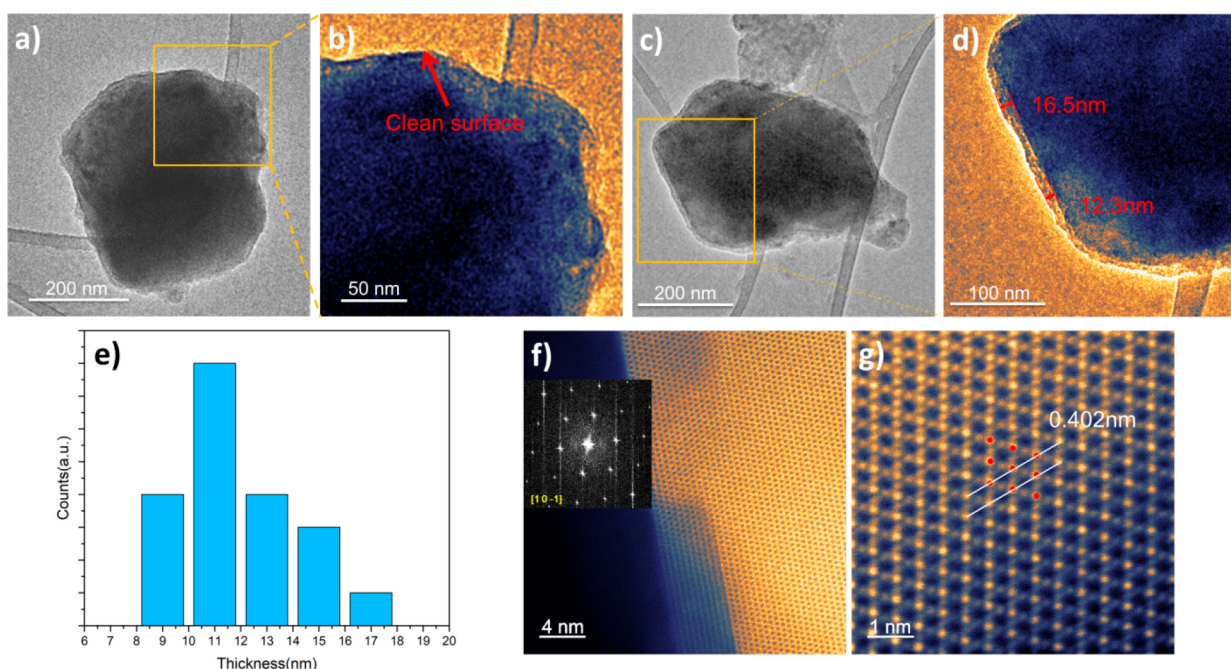
Figure 4. Morphological investigation on LTO at different states of discharge via microscopy: (a, b) TEM images of LTO at 1 V on first discharge, (c, d) TEM images of LTO at 0.01 V on first discharge, (e) the statistic results of SEI thickness on the surface of LTO at 0.01 V on first discharge, and (f, g) atomic-resolution HAADF-STEM from close to the $[10\bar{1}]$ zone axis of LTO at 0.01 V on the first discharge.

Scheme 1. Schematic of the Energy Storage Mechanism of the LTO
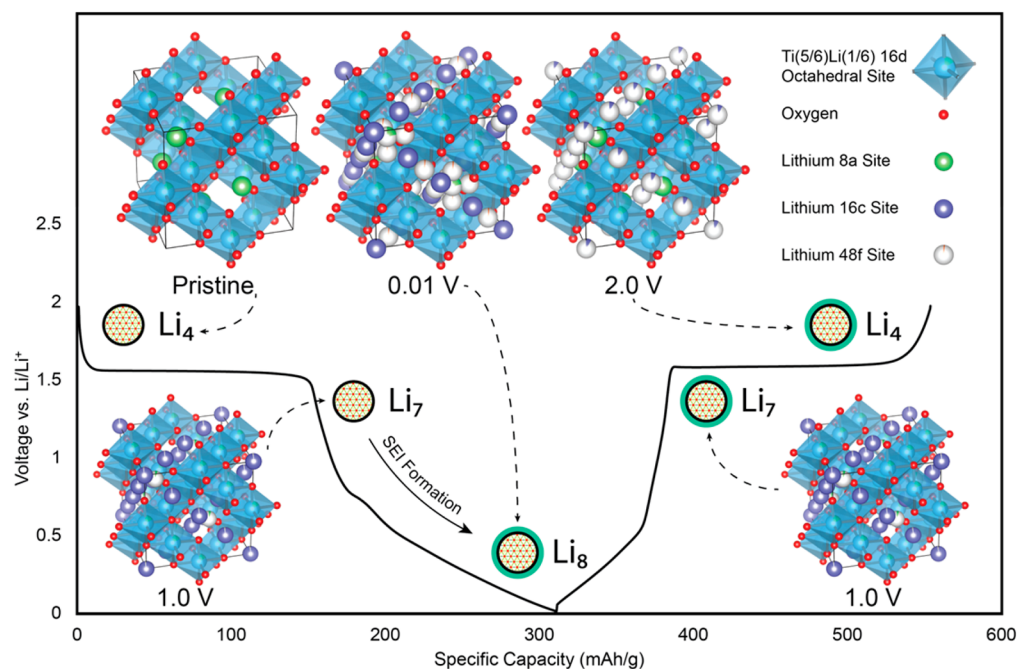
voltage for 3 Li atoms inserted into the structure, computed using the HSE06 functional (1.57 V vs Li/Li⁺), is in excellent agreement with well-known experimental LTO voltage between $Li_4Ti_5O_{12}$ and $Li_7Ti_5O_{12}$ (1.55 V vs Li/Li⁺).[27,28] We note that the voltage profile computed using the metastable cycled $Li_4Ti_5O_{12}$ is in much better agreement, compared to that computed using the pristine $Li_4Ti_5O_{12}$, further supporting the results of the LTO neutron diffraction. When discharging to a very low voltage of 0.01 V, an additional Li can be intercalated into LTO with reversible capacity up to 233 mAh

g⁻¹. The computed voltage for this additional Li insertion from $Li_7Ti_5O_{12}$ to $Li_8Ti_5O_{12}$ is 0.19 V, which is, again, in excellent agreement with the 0.21 V value that is obtained from the reversible voltage profile after stable SEI formation.

In order to investigate the charge compensation mechanism during Li-ion insertion and extraction, X-ray absorption spectroscopy (XAS) measurements were conducted with Ti K-edge at different states of (dis)charge. Normalized Ti K-edge X-ray absorption near-edge structure (XANES) spectra are shown in Figure 3a. There are three characteristic regions in

the spectra: the pre-edge peaks at ~4969 eV, shoulder peaks at ~4975 eV, and peaks at ~4986 eV. It is evident that the pristine $Li_4Ti_5O_{12}$ compound predominantly consists of Ti^{4+}.[29] Clear changes are shown in the Ti XANES spectra upon the discharge and charge process. The Ti K-edge pre-edge intensity is reduced after the lithiation plateau, suggesting that the oxidation state of Ti at 1.0 V is lower than Ti^{4+}.[30] An evident shift of the absorption energy to the lower energy region is observed in the LTO at 0.01 V, compared to that of the pristine state. The amount of absorption energy shift is ~2 eV, suggesting that the oxidation state of Ti is further reduced. After the first charge, the oxidation state of Ti returns to tetravalent. Based on the Ti XANES, it is proved that Ti is the only electrochemically active species. We can also demonstrate Ti reduction (from Ti^{4+} to Ti^{3+}) in the lithiation process through the averaged integrated spin density for Ti from our DFT calculations[31] in Figure 3b. Ti^{4+}, which has the $3d^04s^0$ electron configuration, has a net spin of 0, while Ti^{3+} has a net spin of 1. For $Li_4Ti_5O_{12}$, all Ti are in the 4+ oxidation state, and, hence, the average integrated spin density is 0. When 3 Li atoms are inserted to form $Li_7Ti_5O_{12}$, 3 Ti atoms are reduced to a valency of 3+, resulting in an average integrated spin density of $\sim^3/_5 = 0.6\ \mu_B$ at a radius of 2.0 Å from Ti. When a further Li is inserted to form $Li_8Ti_5O_{12}$, 4 Ti atoms are in the 3+ oxidation state, resulting in an average integrated spin density of $^4/_5 = 0.8\ \mu_B$ at the same radius.

The neutron diffraction results show that only 4 Li atoms intercalate into the LTO during the first discharge, implying the irreversible capacity loss during the first cycle is associated with the side reactions between the electrode and electrolyte, especially at the surface of the electrode. High-resolution transmission electron microscopy was used to examine the LTO discharged to different voltages. Figures 4a and 4b show the low-magnification TEM images of the LTO at 1 V. The LTO particle is ~500 nm with a clean surface. In comparison, Figures 4c and 4d show that the LTO at 0.01 V is covered by an amorphous SEI layer with a thickness of 12 nm. Figure 4e is a statistical investigation of the SEI layers. The thickness of the SEI ranges from 9 nm to 17 nm. The formation of the SEI is irreversible, which is related to the bump at ~0.8 V in the first discharge profile. Consequently, the generation of SEI is responsible for the first cycle capacity loss. It is also possible that some electrolyte-related side reactions occur on the conductive carbon. Figures 4f and 4g depict the atomic-resolution high-angle annular dark-field scanning transmission electron microscopy (HAADF-STEM) of $Li_8Ti_5O_{12}$. The presented images were measured from close to the $[10\bar{1}]$ zone axis. The fast Fourier transform (FFT) result shows that the particle maintains a spinel structure, which is consistent with the neutron diffraction data.

Scheme 1 summarizes our understanding on the working mechanisms of the LTO. The structure of the pristine LTO is $[Li_3]^{8a}[Li_1Ti_5]^{16d}[O_{12}]^{32e}$, which is consistent with the previous literature.[32] After the 1.55 V plateau in the discharge, $Li_4Ti_5O_{12}$ transforms to $[Li_{0.16}]^{8a}[Li_1Ti_5]^{16d}[Li_{5.84}]^{16c}[O_{12}]^{32e}$. Besides, the 3 Li atoms enter the 16c sites in the LTO crystal, the Li also move from the original 8a sites to the 16c sites. Continued discharging of LTO to 0.01 V not only takes one extra Li into the LTO bulk, but also promotes electrolyte reduction at the LTO surface to form a thick SEI layer. The fully discharged LTO is noted as $[Li_{0.62}]^{8a}[Li_1Ti_5]^{16d}[Li_6]^{16c}[Li_{0.38}]^{48f}[O_{12}]^{32e}$, with 8a and 48f sites being partially occupied. Once the LTO is charged back to 1.0 V, its structure recovers to exactly the same

as it is discharged to 1.0 V. The fully delithiated LTO does not return to the pristine structure, with a fraction of Li staying at the 16c sites $([Li_{2.57}]^{8a}[Li_1Ti_5]^{16d}[Li_{0.43}]^{16c}[O_{12}]^{32e})$. The volume change of the LTO unit cell is small during the entire process, and the transformation between $Li_4Ti_5O_{12}$ and $Li_8Ti_5O_{12}$ is highly reversible, which leads to its excellent cycling stability. The charge transfer during the Li (de)-intercalation is compensated by the Ti^{3+}/Ti^{4+} redox.

By using a combination of electrochemical and structural characterization methods, we have identified the charge storage mechanism in LTO, particularly when cycled to 0.01 V. Quantitative analysis of neutron diffraction data identified the limit of Li insertion into the LTO spinel to be 4, with very minor changes in the lattice parameters, which led to highly reversible electrochemical performance. The robustness of the host structure is confirmed by TEM studies. Ti is the sole redox species involved in the charge storage reactions, as confirmed by XANES studies and average integrated spin from simulations. We used DFT calculations to confirm the feasibility of structural difference between pristine and cycled LTO, and the voltage profile calculated by the HSE06 functional is very close to the experimental one. The irreversible capacity loss in its first cycle is caused by the thick SEI formation. The statistic TEM studies show an amorphous SEI layer with thickness of ~12 nm. Our work clearly established that reversible intercalation reactions in oxides are possible at potentials close to Li. The insight may be used to design and optimize other intercalation-type anode materials.

■ ASSOCIATED CONTENT

Ⓢ Supporting Information

The Supporting Information is available free of charge on the ACS Publications website at DOI: 10.1021/acsmaterial-slett.9b00099.

> Experimental methods (synthesis of LTO, electro-chemical tests, neutron diffraction, XAS spectra and STEM); DFT calculations; neutron diffraction and refined data of LTO (PDF)
> Crystallographic data for $Li_4Ti_5O_{12}$ (CIF)
> Crystallographic data for $Li_8Ti_{10}O_{24}$ (CIF)
> Crystallographic data for $Li_4Ti_{10}O_{24}$ (CIF)
> Crystallographic data for $Li_{16}Ti_{10}O_{24}$ (CIF)

■ AUTHOR INFORMATION

Corresponding Authors

*E-mail: huolinx@uci.edu (H. Xin).
*E-mail: ongsp@eng.ucsd.edu (S. P. Ong).
*E-mail: piliu@eng.ucsd.edu (P. Liu).

ORCID Ⓞ

Zhuoying Zhu: 0000-0003-1775-7651
Jason Huang: 0000-0002-6387-1650
Shyue Ping Ong: 0000-0001-5726-2587
Ping Liu: 0000-0002-1488-1668

Author Contributions

∇These authors contributed equally to this work.

Notes

■ REFERENCES

(1) Yuan, T.; Tan, Z. P.; Ma, C. R.; Yang, J. H.; Ma, Z. F.; Zheng, S. Y. Challenges of Spinel $Li_4Ti_5O_{12}$ for Lithium-Ion Battery Industrial Applications. *Adv. Energy Mater.* 2017, 7, 1601625.

(2) Hao, X. G.; Bartlett, B. M. $Li_4Ti_5O_{12}$ Nanocrystals Synthesized by Carbon Templating from Solution Precursors Yield High Performance Thin Film Li-Ion Battery Electrodes. *Adv. Energy Mater.* 2013, 3, 753−761.

(3) Ohzuku, T.; Ueda, A.; Yamamoto, N. Zero-Strain Insertion Material of $Li[Li_{1/3}Ti_{5/3}]O_4$ for Rechargeable Lithium Cells. *J. Electrochem. Soc.* 1995, 142, 1431−1435.

(4) Aravindan, V.; Lee, Y. S.; Madhavi, S. Research Progress on Negative Electrodes for Practical Li-Ion Batteries: Beyond Carbonaceous Anodes. *Adv. Energy Mater.* 2015, 5, 1402225.

(5) Zhao, B. T.; Deng, X.; Ran, R.; Liu, M. L.; Shao, Z. P. Facile Synthesis of a 3D Nanoarchitectured $Li_4Ti_5O_{12}$ Electrode for Ultrafast Energy Storage. *Adv. Energy Mater.* 2016, 6, 1500924.

(6) Han, X.; Gui, X.; Yi, T. F.; Li, Y. W.; Yue, C. B. Recent progress of $NiCo_2O_4$-based anodes for high-performance lithium-ion batteries. *Curr. Opin. Solid State Mater. Sci.* 2018, 22, 109−126.

(7) Yi, T. F.; Zhu, Y. R.; Tao, W.; Luo, S.; Xie, Y.; Li, X. F. Recent advances in the research of $MLi_2Ti_6O_{14}$ (M=2Na, Sr, Ba, Pb) anode materials for Li-ion batteries. *J. Power Sources* 2018, 399, 26−41.

(8) Pang, W. K.; Peterson, V. K.; Sharma, N.; Shiu, J. J.; Wu, S. H. Lithium Migration in $Li_4Ti_5O_{12}$ Studied Using in Situ Neutron Powder Diffraction. *Chem. Mater.* 2014, 26, 2318−2326.

(9) Odziomek, M.; Chaput, F.; Rutkowska, A.; Swierczek, K.; Olszewska, D.; Sitarz, M.; Lerouge, F.; Parola, S. Hierarchically structured lithium titanate for ultrafast charging in long-life high capacity batteries. *Nat. Commun.* 2017, 8, 1−7.

(10) Yi, T. F.; Yang, S. Y.; Xie, Y. Recent advances of $Li_4Ti_5O_{12}$ as a promising next generation anode material for high power lithium-ion batteries. *J. Mater. Chem. A* 2015, 3, 5750−5777.

(11) Yi, T. F.; Xie, Y.; Zhu, Y. R.; Zhu, R. S.; Shen, H. Y. Structural and thermodynamic stability of $Li_4Ti_5O_{12}$ anode material for lithium-ion battery. *J. Power Sources* 2013, 222, 448−454.

(12) Yi, T. F.; Xie, Y.; Wu, Q. J.; Liu, H. P.; Jiang, L. J.; Ye, M. F.; Zhu, R. S. High rate cycling performance of lanthanum-modified $Li_4Ti_5O_{12}$ anode materials for lithium-ion batteries. *J. Power Sources* 2012, 214, 220−226.

(13) Wang, F.; Wu, L. J.; Ma, C.; Su, D.; Zhu, Y. M.; Graetz, J. Excess lithium storage and charge compensation in nanoscale $Li_{4+x}Ti_5O_{12}$. *Nanotechnology* 2013, 24, 424006.

(14) Ge, H.; Li, N.; Li, D. Y.; Dai, C. S.; Wang, D. L. Study on the Theoretical Capacity of Spinel Lithium Titanate Induced by Low-Potential Intercalation. *J. Phys. Chem. C* 2009, 113, 6324−6326.

(15) Chen, Y.; Rangasamy, E.; Liang, C. D.; An, K. Origin of High Li^+ Conduction in Doped $Li_7La_3Zr_2O_{12}$ Garnets. *Chem. Mater.* 2015, 27, 5491−5494.

(16) Liu, X.; Chen, Y.; Hood, Z. D.; Ma, C.; Yu, S.; Sharafi, A.; Wang, H.; An, K.; Sakamoto, J.; Siegel, D. J.; Cheng, Y.; Jalarvo, N. H.; Chi, M. Elucidating the mobility of H^+ and Li^+ ions in $(Li_{6.25−x}H_xAl_{0.25})La_3Zr_2O_{12}$ via correlative neutron and electron spectroscopy. *Energy Environ. Sci.* 2019, 12, 945−951.

(17) Liu, H. D.; Liu, H.; Seymour, I. D.; Chernova, N.; Wiaderek, K. M.; Trease, N. M.; Hy, S.; Chen, Y.; An, K.; Zhang, M. H.; Borkiewicz, O. J.; Lapidus, S. H.; Qiu, B.; Xia, Y. G.; Liu, Z. P.; Chupas, P. J.; Chapman, K. W.; Whittingham, M. S.; Grey, C. P.; Meng, Y. S. Identifying the chemical and structural irreversibility in $LiNi_{0.8}Co_{0.15}Al_{0.05}O_2$ - a model compound for classical layered intercalation. *J. Mater. Chem. A* 2018, 6, 4189−4198.

(18) Liu, H.; Liu, H. D.; Lapidus, S. H.; Meng, Y. S.; Chupas, P. J.; Chapman, K. W. Sensitivity and Limitations of Structures from X-ray and Neutron-Based Diffraction Analyses of Transition Metal Oxide Lithium-Battery Electrodes. *J. Electrochem. Soc.* 2017, 164, A1802−A1811.

(19) Liu, H. D.; Chen, Y.; Hy, S.; An, K.; Venkatachalam, S.; Qian, D. N.; Zhang, M. H.; Meng, Y. S. Operando Lithium Dynamics in the Li-Rich Layered Oxide Cathode Material via Neutron Diffraction. *Adv. Energy Mater.* 2016, 6, 1502143.

(20) Liu, H. D.; Fell, C. R.; An, K.; Cai, L.; Meng, Y. S. In-situ neutron diffraction study of the $xLi_{(2)}MnO_{(3)}$center dot$(1-x)LiMO_2$ (x=0, 0.5; M = Ni, Mn, Co) layered oxide compounds during electrochemical cycling. *J. Power Sources* 2013, 240, 772−778.

(21) Zhang, Q. Y.; Verde, M. G.; Seo, J. K.; Li, X.; Meng, Y. S. Structural and electrochemical properties of Gd-doped Li4Ti5O12 as anode material with improved rate capability for lithium-ion batteries. *J. Power Sources* 2015, 280, 355−362.

(22) Ariyoshi, K.; Yamamoto, S.; Ohzuku, T. Three-volt lithium-ion battery with $Li[Ni_{1/2}Mn_{3/2}]O_4$ and the zero-strain insertion material of $Li[Li_{1/3}Ti_{5/3}]O_4$. *J. Power Sources* 2003, 119, 959−963.

(23) Perdew, J. P.; Burke, K.; Ernzerhof, M. Generalized gradient approximation made simple. *Phys. Rev. Lett.* 1996, 77, 3865−3868.

(24) Zhu, Z. Y.; Chu, I. H.; Ong, S. P. $Li_3Y(PS_4)_{(2)}$ and $Li_5PS_4Cl_2$: New Lithium Superionic Conductors Predicted from Silver Thiophosphates using Efficiently Tiered Ab Initio Molecular Dynamics Simulations. *Chem. Mater.* 2017, 29, 2474−2484.

(25) Chevrier, V. L.; Ong, S. P.; Armiento, R.; Chan, M. K. Y.; Ceder, G. Hybrid density functional calculations of redox potentials

and formation energies of transition metal compounds. *Phys. Rev. B: Condens. Matter Mater. Phys.* **2010**, *82*, 075122.

(26) Heyd, J.; Scuseria, G. E.; Ernzerhof, M. Hybrid functionals based on a screened Coulomb potential. *J. Chem. Phys.* **2003**, *118*, 8207−8215.

(27) Chen, S.; Xin, Y. L.; Zhou, Y. Y.; Ma, Y. R.; Zhou, H. H.; Qi, L. M. Self-supported $Li_4Ti_5O_{12}$ nanosheet arrays for lithium ion batteries with excellent rate capability and ultralong cycle life. *Energy Environ. Sci.* **2014**, *7*, 1924−1930.

(28) Shi, Y.; Tang, H. M.; Jiang, S. L.; Kayser, L. V.; Li, M. Q.; Liu, F.; Ji, F.; Lipomi, D. J.; Ong, S. P.; Chen, Z. Understanding the Electrochemical Properties of Naphthalene Diimide: Implication for Stable and High-Rate Lithium-Ion Battery Electrodes. *Chem. Mater.* **2018**, *30*, 3508−3517.

(29) Kim, C.; Yu, Y. S.; Moyon, B.; Sirisopanaporn, C.; Richardson, T. J.; Cabana, J. Visualization of the Phase Propagation within Carbon-Free $Li_4Ti_5O_{12}$ Battery Electrodes. *J. Phys. Chem. C* **2016**, *120*, 29030−29038.

(30) Zhang, W.; Topsakal, M.; Cama, C.; Pelliccione, C. J.; Zhao, H.; Ehrlich, S.; Wu, L. J.; Zhu, Y. M.; Frenkel, A. I.; Takeuchi, K. J.; Takeuchi, E. S.; Marschilok, A. C.; Lu, D. Y.; Wang, F. Multi-Stage Structural Transformations in Zero-Strain Lithium Titanate Unveiled by in Situ X-ray Absorption Fingerprints. *J. Am. Chem. Soc.* **2017**, *139*, 16591−16603.

(31) Feng, X. Y.; Chien, P. H.; Zhu, Z. Y.; Chu, I. H.; Wang, P. B.; Immediato-Scuotto, M.; Arabzadeh, H.; Ong, S. P.; Hu, Y. Y. Studies of Functional Defects for Fast Na-Ion Conduction in $Na_{3-y}PS_{4-x}Cl_x$ with a Combined Experimental and Computational Approach. *Adv. Funct. Mater.* **2019**, *29*, 1807951.

(32) Verde, M. G.; Baggetto, L.; Balke, N.; Veith, G. M.; Seo, J. K.; Wang, Z. Y.; Meng, Y. S. Elucidating the Phase Transformation of $Li_4Ti_5O_{12}$ Lithiation at the Nanoscale. *ACS Nano* **2016**, *10*, 4312−4321.